Increased Stability of Low-Speed Turning Through a Distributed Force and Continuous Delay Model

Firas A. Khasawneh[1]
e-mail: firas.khasawneh@duke.edu

Brian P. Mann

Department of Mechanical Engineering and
Materials Science,
Duke University,
Durham, NC 27708

Tamás Insperger

Gabor Stépán

Department of Applied Mechanics,
Budapest University of Technology and
Economics,
H-1521 Budapest, Hungary

This paper investigates the increased stability behavior commonly observed in low-speed machining. In the past, this improved stability has been attributed to the energy dissipated by the interference between the workpiece and the tool relief face. In this study, an alternative physical explanation is described. In contrast to the conventional approach, which uses a point force acting at the tool tip, the cutting forces are distributed over the tool-chip interface. This approximation results in a second-order delayed integrodifferential equation for the system that involves a short and a discrete delay. A method for determining the stability of the system for an exponential shape function is described, and temporal finite element analysis is used to chart the stability regions. Comparisons are then made between the stability charts of the point force and the distributed force models for continuous and interrupted turning. [DOI: 10.1115/1.3187153]

Keywords: continuous delay, distributed delay, process damping, stability, temporal finite elements analysis, time delay, turning

1 Introduction

The relative vibrations between the tool and the workpiece are a normal phenomenon associated with cutting operations. When these vibrations become unstable, they are commonly referred to as chatter, which may result in inferior part surfaces and increased tool wear. Chatter can also damage the workpiece, the fixture, and/or the machine spindle. Mapping the areas of stability as a function of the machining parameters, namely, the depth of cut and the spindle speed, not only helps avoid these detrimental effects of chatter but also increases the efficiency of the cutting process. Predictive models that can generate stability regions for a wide combination of speeds and cutting depths eliminate the costly and time-consuming trial and error alternative.

In order to generate the stability charts for a cutting operation, it is necessary to model the system dynamics through suitable equations of motion, descriptive force models, and then apply proper solution techniques. Models describing cutting tool vibrations began to appear in literature about half a century ago [1–4]. Several models have been proposed to characterize the cutting forces as a function of the cutting parameters, such as the depth of cut and the instantaneous chip thickness whose product forms the instantaneous chip area. These models treated cutting forces as a point force acting at the tool tip. This conventional approximation of the cutting forces has been verified experimentally in the middle range of cutting speeds. However, actual observations of the cutting process at low speeds show improved stability when compared with those obtained from theoretical predictions (e.g., see Fig. 1).

There are many machining operations that can be performed only at low speeds. For instance, materials which are harder to machine, such as stainless steel and titanium, are used extensively in medical tool manufacturing and in the aerospace industry. Titanium, for example, has very high strength to weight ratio and

excellent corrosion resistance, which makes it ideal for aerospace applications [5]. Titanium also has great biocompatibility so it is widely used in medical implants [6]. However, titanium is difficult to machine owing to its inherent properties of high strength combined with poor thermal conductivity. This requires titanium to be machined only at low speeds.

The improved stability behavior at low speeds has been attributed to an energy dissipation mechanism commonly called process damping. Process damping plays a key role in stability determination in machining processes [7–9]. Tobias and Fishwick [1], Tlusty [10], and Minis et al. [11] tried to account for process damping by including the displacement variable and its derivative in the cutting force model. Other models recognized process damping as the result of the interference between the cutting tool flank face and the undulated machined surface [7], where the amplitude of the force was assumed to be proportional to the material volume displaced due to interference [12–16]. Chiou and Liang [17] and later Clancy and Shin [18] used this model to account for process damping to capture the effect of tool wear on stability in turning. The same model was implemented by Chandiramani and Pothala [19] in their study of regenerative chatter in a two degree of freedom model for turning.

An alternative explanation for the increased stability at lower speeds was recently introduced by Stépán [20,21]. Instead of modeling the cutting forces as a single point force, a continuous or distributed time delay model was introduced to capture the force distribution over the tool-chip interface (see Fig. 2). This paper investigates the influence of the distributed force model on the stability behavior of continuous and interrupted turning. In particular, we describe an approach to transform the distributed delay equations into a discrete delay system. Theoretical stability investigations were performed using a state-space temporal finite element analysis (TFEA) technique [22]. Finally, different continuous-to-discrete delay ratios are used to elucidate parameter regimes where the phenomenological increased stability behavior is adequately captured.
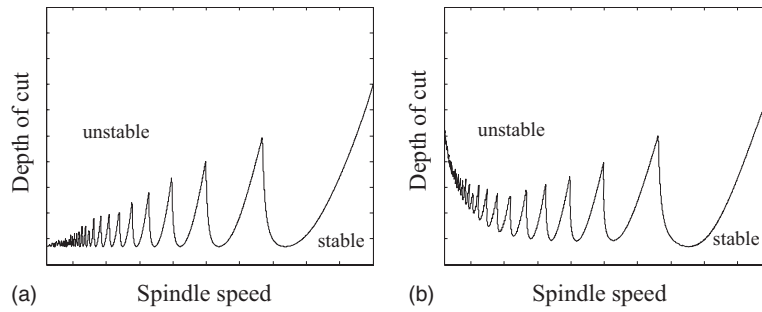
Fig. 1 Qualitative stability charts shown to illustrate the phenomenological increase in stability at relatively low cutting speeds. Graph (a) shows the stability boundaries for a typical point force model and graph (b) provides a qualitative representation of the commonly observed stability increase at low speeds.

2 Turning Process Models

This section starts by deriving a variational equation of motion for a single degree of freedom turning process. In Sec. 2.2, the conventional point force model is described and the corresponding variational equation of motion is obtained. The resulting equation is then nondimensionalized and is written into its state-space form, which is used for stability determination. In Sec. 2.3, the distributed force model is introduced and the corresponding variational equation of motion is derived. This equation includes the discrete time delay, due to the tool passage period, as well as a continuous time delay due to the chip sliding over the tool-chip interface.

2.1 Equation of Motion. The governing equation of motion for a rigid workpiece and a tool compliant in one direction, $z(t)$, is

$$m\ddot{z} + c\dot{z} + kz = -F_z(A) \tag{1}$$

where m, c, and k are the modal mass, stiffness, and damping, respectively, and $F_z(A)$ is the cutting force component along the z direction as a function of the instantaneous chip area, $A(t)$. The instantaneous chip area is the product of the depth of cut, b, and the instantaneous chip thickness, $h(t)$, i.e., $A(t)=bh(t)$.

Let z^* be the equilibrium solution for the system, which corresponds to cutting at the nominal depth of cut h_o. Under these conditions, the system is in equilibrium with the static cutting force, f_o. Then for any other solution, $z(t)$ [23], one can write
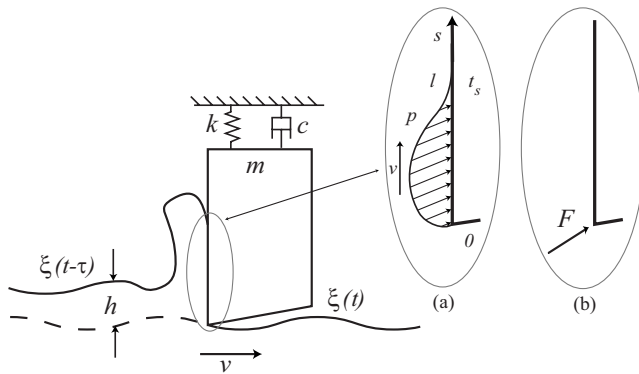

Fig. 2 Schematic diagram of a: (a) distributed force model and (b) conventional point force model. Case (a) uses a stress distribution over the tool rake face and applies a finite time for the chip to travel along the tool-chip interface. Case (b) is the conventional modeling approach of using a point force and a discrete delay model.

$$z(t) = z^* + \xi(t) \tag{2}$$

where $\xi(t)$ represents a perturbation of the equilibrium solution. The growth or decay of such small perturbations determines the stability of the original system, Eq. (1). Similarly, the cutting force can be described as the summation of a static component and a dynamic variation due to oscillations

$$F_z(A) \approx f_o + \Delta F_z(A) \tag{3a}$$

$$\approx -kz^* + \Delta F_z(A) \tag{3b}$$

Equations (2) and (3) are substituted into Eq. (1) to obtain the variational equation

$$m\ddot{\xi}(t) + c\dot{\xi}(t) + k\xi(t) \approx -\Delta F_z(A) \tag{4}$$

Dropping the approximation sign and dividing by the mass, m, Eq. (4) becomes

$$\ddot{\xi}(t) + 2\zeta\omega_n\dot{\xi}(t) + \omega_n^2\xi(t) = -\frac{1}{m}\Delta F_z(A) \tag{5}$$

where $\omega_n = \sqrt{k/m}$ is the angular natural frequency, $\zeta = c/(2m\omega_n)$ is the damping ratio, and $\Delta F_z(A)$ is the dynamic force variation. The expression for the force variation depends on the adopted force model and the type of cutting, i.e., continuous or interrupted. In Sec. 2.2, the conventional point force model will be used in conjunction with Eq. (5) to produce an equation that can be used to determine the stability regions.

2.2 Point Force Model. In the conventional point force model, cutting forces are characterized by a single force vector acting at a single point—the tool tip. This force is assumed to be a function of the instantaneous chip area, $A(t)$ (see Fig. 3).
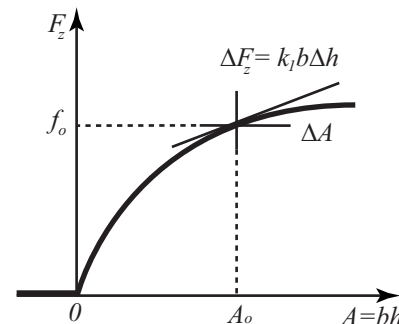

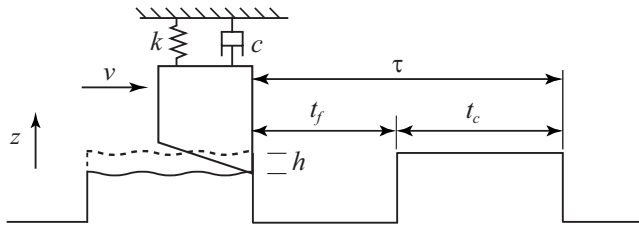**Fig. 3 Cutting force and chip area relation**

Fig. 4 Schematic diagram of the interrupted cutting process. The force is proportional to the uncut chip area when the tool is in contact with the work piece but drops to zero when the tool vibrates freely [31].

The dynamic force variation is written as a Taylor series expansion around the nominal uncut chip area A_o

$$\Delta F_z(A) = u(t)(F_z(A) - f_o) = u(t)\sum_{j=1}^{p} k_j(\Delta A)^j \qquad (6)$$

where for continuous turning the tool is assumed to be in the cut all the time and $u(t)$ assumes a value of one, i.e., $u(t)=1$. In contrast to continuous turning, interrupted turning is a piecewise continuous system where the tool is not always cutting but enters and exits the cut, Fig. 4. When the tool is in the cut, a force proportional to the uncut chip area acts on the tool. However, when the tool exits the cut, the system will undergo free vibration (i.e., for interrupted turning, $u(t)$ is a switching function: its value is 1 when the tool is cutting and 0 when the tool exits the cut). The chip area variation is

$$\Delta A = A - A_o = b(h - h_o) \qquad (7)$$

The coefficients of the power series in Eq. (6) come from

$$k_j = \frac{1}{j!}\frac{d^j F_z(A_o)}{dA^j}, \quad j=1,2,\ldots \qquad (8a)$$

$$\Rightarrow \{k_j\} = \{k_1,k_2,k_3,\ldots\} = \left\{ \frac{df(A_o)}{dA}, \frac{1}{2!}\frac{d^2 f(A_o)}{dA^2}, \frac{1}{3!}\frac{d^3 f(A_o)}{dA^3}, \ldots \right\} \qquad (8b)$$

The first coefficient, k_1, in the above expression is referred to as the cutting coefficient and is usually determined experimentally. k_1 represents the linear approximation of the cutting force variation, while the higher order terms, $k_2 - k_\infty$, provide higher order approximations.

The linear approximation of the cutting force variation is inserted into Eq. (5) to obtain

$$\ddot{\xi}(t) + 2\zeta\omega_n\dot{\xi}(t) + \omega_n^2\xi(t) = -u(t)\frac{k_1 b}{m}(h(t) - h_o) \qquad (9)$$

Substituting $h(t)=h_o+\xi(t)-\xi(t-\tau)$ into Eq. (9) gives

$$\ddot{\xi}(t) + 2\zeta\omega_n\dot{\xi}(t) + \omega_n^2\xi(t) = -u(t)\frac{k_1 b}{m}(\xi(t) - \xi(t-\tau)) \qquad (10)$$

which represents a delay differential equation (DDE) with constant coefficients.

A set of dimensionless parameters for time, spindle speed, time delay, and depth of cut [24] is defined as

$$\tilde{t} = \omega_n t \qquad (11a)$$

$$\tilde{\Omega} = \frac{\Omega}{\omega_n} \qquad (11b)$$

$$\tilde{\tau} = \omega_n \tau \qquad (11c)$$

$$\tilde{b} = \frac{bk_1}{m\omega_n^2} \qquad (11d)$$

These substitutions result in the dimensionless characteristic frequency $\tilde{\omega}_n=1$. The nondimensionalized version of Eq. (10) then reads

$$\ddot{\xi}(\bar{t}) + 2\zeta\dot{\xi}(\bar{t}) + \xi(\bar{t}) = -u(t)\tilde{b}(\xi(\bar{t}) - \xi(\bar{t} - \tilde{\tau})) \qquad (12)$$

Equation (12) can be written in state-space form as

$$\begin{bmatrix} \dot{x}_1 \\ \dot{x}_2 \end{bmatrix} = \begin{bmatrix} 0 & 1 \\ -(u(t)\tilde{b}+1) & -2\zeta \end{bmatrix}\begin{bmatrix} x_1 \\ x_2 \end{bmatrix} + \begin{bmatrix} 0 & 0 \\ u(t)\tilde{b} & 0 \end{bmatrix}\begin{bmatrix} x_1(t-\tau) \\ x_2(t-\tau) \end{bmatrix}$$
$$(13)$$

where the tilde was dropped from t and τ for convenience. To help explain the analysis that follows, the above state-space equation is written in a more compact form

$$\dot{\mathbf{x}}(t) = \mathbf{A}(t)\mathbf{x}(t) + \mathbf{B}(t)\mathbf{x}(t-\tau) \qquad (14)$$

Equation (14) describes a turning operation subject to the conventional point force model. The stability analysis of equations having the same form as Eq. (14) will be explained using the state-space temporal finite element approach, TFEA, in Sec. 3 (see Ref. [22]). In Sec. 2.3, an analogous equation will be formulated for the distributed force model.

2.3 Distributed Force Model. The distributed force model reflects a more realistic representation of the physical cutting forces in turning. Instead of concentrating the cutting forces at a single point, these forces are assumed to have a distribution per unit length P_z with varying magnitudes along the tool-chip interface. The cutting forces can be described in terms of this distribution by

$$F_z(A) = \int_0^l P_z(A,s)ds \qquad (15)$$

where s is a local coordinate whose origin is fixed to the tool tip. This local coordinate describes the contact distance between the sliding chip and the active face of the tool. The range of values for s is from 0 to the length, which represents the location where the chip separates from the tool l. One approximation for P_z combines the Taylor approximation of the cutting force with an estimated shape function W (with units of 1/m)

$$P_z(A,s) = F_z(A)W(s), \quad s \in [0,l] \qquad (16)$$

In order to ensure that this new model maintains the mechanics of the system, substituting $A=A_o$, which corresponds to cutting under stationary conditions, should yield a value of $f_o=F_z(A_o)$. Imposing this constraint on Eq. (15) gives

$$F_z(A_o) = \int_0^l P_z(A_o,s)ds = F_z(A_o)\int_0^l W(s)ds$$

$$\Rightarrow \int_0^l W(s)ds = 1 \qquad (17)$$

Equation (17) provides a fundamental condition, which has to be satisfied by any chosen shape function. Let τ be the discrete time delay associated with the tool passage period, and let the short time delay t_s be the time the chip is in contact with the tool. These two different delays are given by

$$\tau = \frac{d_o\pi}{v} = \frac{2\pi}{\Omega}, \quad t_s = \frac{l}{v_c} = \frac{l}{r_c v} \qquad (18)$$

where $d_o\pi$ is the circumference of the cylindrical workpiece, Ω is the angular velocity of the workpiece in units of rad/s, r_c is the chip thickness ratio, and $v_c=r_c v$ is the chip speed over the rake
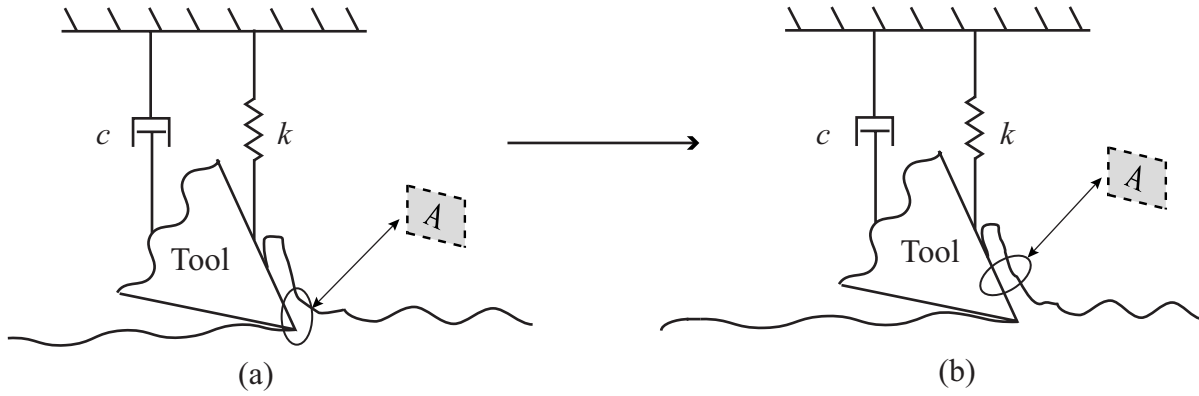
Fig. 5 Short time delay embedding into the force model. The area of a certain segment of the chip flowing over the rake face in (b) can be described by the area of the same segment as it was being cut at the tool tip in (a) at time $t - \hat{t}$.

face [25]. It follows that the ratio of the short time delay t_s to the long one τ is constant

$$r = \frac{t_s}{\tau} = \frac{l}{r_c d_o \pi}$$

The shape of the stress distribution can be expressed in the time domain by introducing a local time $\hat{t} = s/v_c$. Substituting $\hat{t}$ into Eq. (17) yields the following condition on the shape function in the local time domain

$$\int_0^l W(s)ds = 1$$

$$\Rightarrow \int_0^{t_s} v_c W(v_c \hat{t})d\hat{t} = 1, \quad \text{let} \quad w(\hat{t}) = v_c W(v_c \hat{t})$$

$$\Rightarrow \int_0^{t_s} w(\hat{t})d\hat{t} = 1 \tag{19}$$

This local time, $\hat{t} \in [0, t_s]$, gives how much earlier in time a certain segment of the chip flowing over the active tool face was being cut at the tip of the tool as shown in Fig. 5. The assumption that the chip flows at a speed $v_c = r_c v$ means that the area of a section of the chip above the tool tip at a local time $\hat{t}$ is equal to the area of the same chip section as it was being cut at the tool tip at $t - \hat{t}$ time units ago or

$$A(t,\hat{t}) = b(h_o + \xi(t - \hat{t}) - \xi(t - \tau - \hat{t})), \quad t \in [t_o, \infty), \quad \hat{t} \in [0, t_s] \tag{20}$$

where $A(t,\hat{t})$ defines the chip area at time t and local time $\hat{t}$. At $\hat{t} = 0$, Eq. (20) gives back the regular expression for the chip area at the tool tip

$$A(t,0) = b(h_o + \xi(t) - \xi(t - \tau))$$

The cutting force distribution can now be expressed in the z direction in the time domain using the global time t and the local one $\hat{t}$

$$p_z(t,\hat{t}) = P_z(A(t,\hat{t}), v_c \hat{t}) = F_z(A(t,\hat{t})) \frac{1}{v_c} w(\hat{t}), \quad t \in [t_o, \infty),$$

$$\hat{t} \in [0, t_s] \tag{21}$$

By substituting the above results, Eqs. (15), (19), and (21), the power series from Eq. (6) and also the chip area from Eq. (20), the cutting force variation in the z direction reads

$$\Delta F_z(A(t,\hat{t})) \approx u(t) \int_0^{t_s} \sum_{j=1}^p k_j b^j (\xi(t - \hat{t}) - \xi(t - \tau - \hat{t}))^j w(\hat{t}) d\hat{t} \tag{22}$$

$$\approx u(t) k_1 b \int_0^{t_s} (\xi(t - \hat{t}) - \xi(t - \tau - \hat{t})) w(\hat{t}) d\hat{t} \tag{23}$$

where Eq. (23) is the expression for the linearized cutting force variation. For continuous turning $u(t) = 1$, thus, substituting Eq. (23) into the variational equation of motion Eq. (5) yields

$$\ddot{\xi} + 2\zeta\omega_n\dot{\xi} + \omega_n^2\xi = -\frac{k_1 b}{m} \int_0^{t_s} (\xi(t - \hat{t}) - \xi(t - \tau - \hat{t})) w(\hat{t}) d\hat{t} \tag{24}$$

The integrodifferential form of Eq. (24) as well as the short time delay complicate the stability analysis of the system. However, Eq. (24) can still be solved through a suitable choice of the weight function. The solution technique involves increasing the order of the system by one and writing the short delay in terms of the discrete one as will be shown in Sec. 3.

3 Stability Analysis

In this section, Eq. (24) is converted into a solvable form through using an exponential weight function. The stability analysis of the resulting state-space equations is then carried out using state-space TFEA. The analysis is shown only for the distributed delay system and a similar analysis can be used for the point force model system, Eq. (14). In Secs. 3.1 and 3.2, stability boundaries are plotted for continuous and interrupted turning, respectively. In each of these sections, the results are shown for both: the point force model and the distributed force model with different continuous-to-discrete delay ratios.

Assume that the shape of the distributed cutting force system $W(s)$ is approximated by the exponential function

$$W(s) = \frac{1}{l} \exp\left(\frac{-s}{l}\right) \Rightarrow w(\hat{t}) = \frac{v_c}{l} \exp\left(\frac{-v_c}{l}\hat{t}\right) = \frac{1}{r\tau} \exp\left(\frac{-\hat{t}}{r\tau}\right),$$

$$\hat{t} \in [0, \infty) \tag{25}$$

This choice of the weight function agrees with several studies, which showed that the normal forces over the rake face vary exponentially [25–29]. Furthermore, the analysis of the DDE described in Eq. (24) is simplified by using this exponential weight function since the distributed delay only increases the system di-

mension by one. The procedure starts with differentiating Eq. (24) with respect to the time t to calculate

$$\overset{(3)}{\xi}(t) + 2\zeta\omega\ddot{\xi}(t) + \omega_n^2\dot{\xi}(t)$$
$$= -\frac{k_1 b}{mr\tau}\int_0^\infty (\dot{\xi}(t-\hat{t}) - \dot{\xi}(t-\tau-\hat{t}))\exp\left(\frac{-\hat{t}}{r\tau}\right)d\hat{t}$$

However, to account for the discontinuous cutting forces during interrupted cutting, the right hand side is multiplied by a switching function, $u(t)$, which gives

$$\overset{(3)}{\xi}(t) + 2\zeta\omega\ddot{\xi}(t) + \omega_n^2\dot{\xi}(t)$$
$$= -u(t)\frac{k_1 b}{mr\tau}\int_0^\infty (\dot{\xi}(t-\hat{t}) - \dot{\xi}(t-\tau-\hat{t}))\exp\left(\frac{-\hat{t}}{r\tau}\right)d\hat{t} \quad (26)$$

where $u(t)$ is 1 for continuous turning and it switches between 0 and 1 for interrupted cutting. Next, the right hand side of Eq. (26) is integrated by parts

$$-u(t)\frac{k_1 b}{mr\tau}\int_0^\infty (\dot{\xi}(t-\hat{t}) - \dot{\xi}(t-\tau-\hat{t}))\exp\left(\frac{-\hat{t}}{r\tau}\right)d\hat{t}$$

$$= u(t)\frac{k_1 b}{mr\tau}\left[(\xi(t-\hat{t}) - \xi(t-\tau-\hat{t}))\exp\left(\frac{-\hat{t}}{r\tau}\right)\right]_0^\infty$$

$$+ u(t)\frac{k_1 b}{mr\tau}\frac{1}{r\tau}\int_0^\infty (\xi(t-\hat{t}) - \xi(t-\tau-\hat{t}))\exp\left(\frac{-\hat{t}}{r\tau}\right)d\hat{t}$$

$$= -u(t)\frac{k_1 b}{mr\tau}(\xi(t) - \xi(t-\tau)) - \frac{1}{r\tau}(\ddot{\xi}(t) + 2\zeta\omega_n\dot{\xi}(t) + \omega_n^2\xi(t))$$
$$\quad (27)$$

Substituting the force expression (27) back into Eq. (24) gives

$$\overset{(3)}{\xi}(t) + \left(\frac{1}{r\tau} + 2\zeta\omega\right)\ddot{\xi}(t) + \left(\frac{2\zeta\omega_n}{r\tau} + \omega_n^2\right)\dot{\xi}(t) + \frac{1}{r\tau}\left(\omega_n^2 + \frac{u(\bar{t})k_1 b}{m}\right)\xi(t)$$
$$- u(\bar{t})\frac{k_1 b}{mr\tau}\xi(t-\tau) = 0, \quad (28)$$

and the equation of motion has been transformed into a third-order system without a continuous time delay but still having the discrete delay τ. Equation (28) can be nondimensionalized using the same parameters introduced in Eq. (11d). This results in the following nondimensional third-order DDE

$$\overset{(3)}{\xi}(\tilde{t}) + \left(\frac{1}{r\tilde{\tau}} + 2\zeta\right)\ddot{\xi}(\tilde{t}) + \left(\frac{2\zeta}{r\tilde{\tau}} + 1\right)\dot{\xi}(\tilde{t}) + \frac{1}{r\tilde{\tau}}(1 + u(\tilde{t})\tilde{b})\xi(\tilde{t})$$
$$- u(\tilde{t})\frac{\tilde{b}}{r\tilde{\tau}}\xi(\tilde{t} - \tilde{\tau}) = 0 \quad (29)$$

which can be written in state-space form as

$$\begin{bmatrix} \dot{y}_1 \\ \dot{y}_2 \\ \dot{y}_3 \end{bmatrix} = \begin{bmatrix} 0 & 1 & 0 \\ 0 & 0 & 1 \\ -\frac{1}{r\tilde{\tau}}(1 + u(t)\tilde{b}) & -\left(\frac{2\zeta}{r\tilde{\tau}} + 1\right) & -\left(\frac{1}{r\tilde{\tau}} + 2\zeta\right) \end{bmatrix} \begin{bmatrix} y_1 \\ y_2 \\ y_3 \end{bmatrix}$$
$$+ \begin{bmatrix} 0 & 0 & 0 \\ 0 & 0 & 0 \\ u(t)\frac{\tilde{b}}{r\tilde{\tau}} & 0 & 0 \end{bmatrix} \begin{bmatrix} y_1(t-\tau) \\ y_2(t-\tau) \\ y_3(t-\tau) \end{bmatrix} \quad (30)$$

where the tilde was dropped from t and τ for convenience. The state-space equation could be written in an equivalent form as

$$\dot{\mathbf{y}}(t) = \mathbf{C}(t)\mathbf{y}(t) + \mathbf{D}(t)\mathbf{y}(t-\tau) \quad (31)$$

The stability analysis of Eq. (31) can be carried out using state-space TFEA approach introduced by Mann and Patel [22]. In this approach, the expressions for the current state and the delayed state variables are written as vectors

$$\mathbf{y}_j(t) = \sum_{i=1}^3 \mathbf{a}_{ji}^n \phi_i(\sigma) \quad (32a)$$

$$\mathbf{y}_j(t-\tau) = \sum_{i=1}^3 \mathbf{a}_{ji}^{n-1} \phi_i(\sigma) \quad (32b)$$

during the jth element. These vectors represent an approximate solution for Eq. (14) in the form of a linear combination of trial functions $\phi_i(\sigma)$. The local time σ varies from zero to the time of each element $t_j = \tau/E$, where E represents the number of elements used in the analysis. The chosen trial functions are orthogonalized on the interval $0 \le \sigma \le t_j$ and the use of the local time notation ensures that they remain orthogonal for every temporal element. The set of polynomial trial functions used for this analysis are

$$\phi_1(\sigma) = 1 - 23\left(\frac{\sigma}{t_j}\right)^2 + 66\left(\frac{\sigma}{t_j}\right)^3 - 68\left(\frac{\sigma}{t_j}\right)^4 + 24\left(\frac{\sigma}{t_j}\right)^5 \quad (33a)$$

$$\phi_2(\sigma) = 16\left(\frac{\sigma}{t_j}\right)^2 - 32\left(\frac{\sigma}{t_j}\right)^3 + 16\left(\frac{\sigma}{t_j}\right)^4 \quad (33b)$$

$$\phi_3(\sigma) = 7\left(\frac{\sigma}{t_j}\right)^2 - 34\left(\frac{\sigma}{t_j}\right)^3 + 52\left(\frac{\sigma}{t_j}\right)^4 - 24\left(\frac{\sigma}{t_j}\right)^5 \quad (33c)$$

The above trial functions are obtained through interpolation, and they are constructed such that the coefficients of the assumed solution directly represent the state variable at the beginning, middle, and end of each temporal element, i.e., at $\sigma=0$, $t_j/2$, and t_j, respectively. The construction and properties of these functions are discussed in more details in Ref. [22]. For demonstration purposes, it is assumed that two elements are sufficient, i.e., $E=2$, then the corresponding form of the assumed solution is substituted into Eq. (14) and using the method of weighted residuals a global matrix can be obtained that relates the states of the system in the current period to those in the previous period

$$\begin{bmatrix} \mathbf{I} & 0 & 0 & 0 & 0 \\ \mathbf{N}_{11}^1 & \mathbf{N}_{12}^1 & \mathbf{N}_{13}^1 & 0 & 0 \\ \mathbf{N}_{21}^1 & \mathbf{N}_{22}^1 & \mathbf{N}_{23}^1 & 0 & 0 \\ 0 & 0 & \mathbf{N}_{11}^2 & \mathbf{N}_{12}^2 & \mathbf{N}_{13}^2 \\ 0 & 0 & \mathbf{N}_{21}^2 & \mathbf{N}_{22}^2 & \mathbf{N}_{23}^2 \end{bmatrix} \begin{bmatrix} a_{11} \\ a_{12} \\ a_{21} \\ a_{22} \\ a_{23} \end{bmatrix}^n$$

$$= \begin{bmatrix} 0 & 0 & 0 & 0 & \mathbf{\Phi} \\ \mathbf{P}_{11}^1 & \mathbf{P}_{12}^1 & \mathbf{P}_{13}^1 & 0 & 0 \\ \mathbf{P}_{21}^1 & \mathbf{P}_{22}^1 & \mathbf{P}_{23}^1 & 0 & 0 \\ 0 & 0 & \mathbf{P}_{11}^2 & \mathbf{P}_{12}^2 & \mathbf{P}_{13}^2 \\ 0 & 0 & \mathbf{P}_{21}^2 & \mathbf{P}_{22}^2 & \mathbf{P}_{23}^2 \end{bmatrix} \begin{bmatrix} a_{11} \\ a_{12} \\ a_{21} \\ a_{22} \\ a_{23} \end{bmatrix}^{n-1} \quad (34)$$

which can be written in a more compact form as

$$\mathbf{H}\mathbf{a}_n = \mathbf{G}\mathbf{a}_{n-1} \quad (35)$$

where $\mathbf{I}$ is an identity matrix and $\mathbf{\Phi}$ depends on the cutting process and the force model used. It is an identity matrix for continuous turning, while for interrupted cutting, it is a state transition matrix (see Appendix). The dimension of $\mathbf{\Phi}$ is 2×2 for the conventional point force model and 3×3 for the distributed force model. The terms $\mathbf{N}_{pi}^j$ and $\mathbf{P}_{pi}^j$ are the following square matrices:

$$\mathbf{N}_{pi}^j = \int_0^{t_j} (\mathbf{I}\dot{\phi}_i(\sigma) - \mathbf{C}\phi_i(\sigma)))\psi_p(\sigma)d\sigma \quad (36a)$$
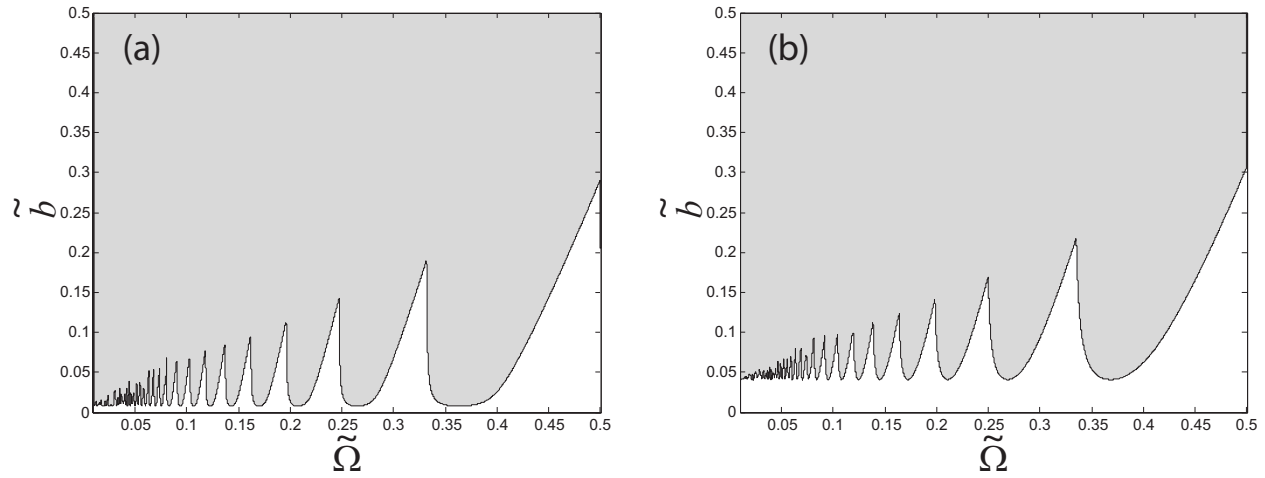
Fig. 6 Stability charts for the point force model of continuous turning plotted as a function of the nondimensionalized cutting speed and depth of cut. The damping ratios used are (*a*) $\zeta=0.0038$ and (*b*) $\zeta=0.02$ (unstable regions shaded).

$$\mathbf{P}^j_{pi} = \int_0^{t_j} (\mathbf{D}\phi_i(\sigma))\psi_p(\sigma)d\sigma \qquad (36b)$$

The functions $\psi_p(\sigma)$ are called test functions or weighting functions. These functions are used to minimize the error incurred from the solution approximation. The weighting functions used for the presented analysis were shifted Legendre polynomials. These polynomials were used because they satisfy the required condition of linear independence. Here, only the first two shifted Legendre polynomials, $\psi_1(\sigma)=1$ and $\psi_2(\sigma)=2(\sigma/t_j)-1$, will be used to keep the resulting matrices square. Recalling that the coefficients of the assumed solution directly represent the state variable at various points in time, Eq. (35) can alternatively be written as

$$\mathbf{y}_n = \mathbf{Q}\mathbf{y}_{n-1} \qquad (37)$$

where $\mathbf{Q}=\mathbf{H}^{-1}\mathbf{G}$ is called the monodromy operator. Equation (37) represents a discrete solution form for Eq. (14) that maps the states of the system over a single delay period from the $n-1$ period to the nth period. Here, the condition for asymptotical stability requires that all the characteristic multipliers, or eigenvalues of $\mathbf{Q}$, must lie within the unit circle of the complex plane. For

more details about this technique, and for convergence properties, the reader can refer to Ref. [22].

In the above analysis, an exponential shape function was assumed to describe the force distribution. Other shape functions were also suggested [21], however, only the exponential one can be transformed into a discrete delay system.

3.1 Continuous Turning Stability. Figure 6 shows two stability charts that were obtained using the point force model. Two cases were considered: one with a relatively high damping ratio, $\zeta=0.02$, and another with a relatively low damping ratio, $\zeta=0.0038$. The region below the boundary line represents stable cutting conditions while that above the boundary line corresponds to an unstable cutting process. It can be seen that at low speeds, this model does not capture the improved stability encountered in practice. For all continuous turning stability plots, a square grid of 600×600 points was used.

Figure 7 shows two stability plots that were obtained with the distributed force model. These plots were generated with a very low value of the delay ratio, $r=0.001$, and they can be compared directly to their counterparts for a point force model in Fig. 6. It can be seen that the distributed force model gives results similar
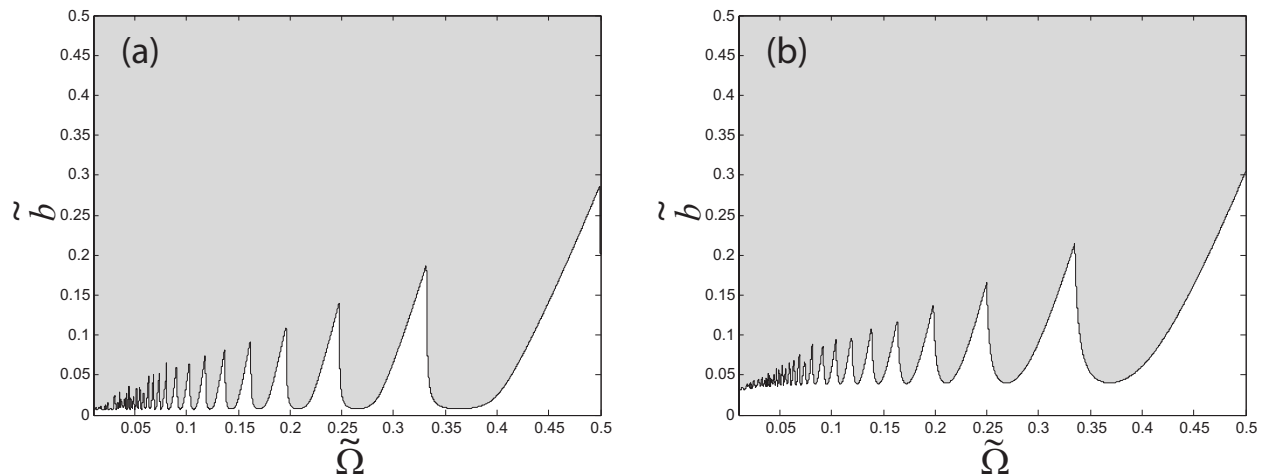

Fig. 7 Stability charts for the distributed force model of continuous turning plotted as a function of the nondimensionalized cutting speed and depth of cut. The delay ratio used is $r=0.001$ and the damping ratios used are (*a*) $\zeta=0.0038$ and (*b*) $\zeta=0.02$ (unstable regions shaded).
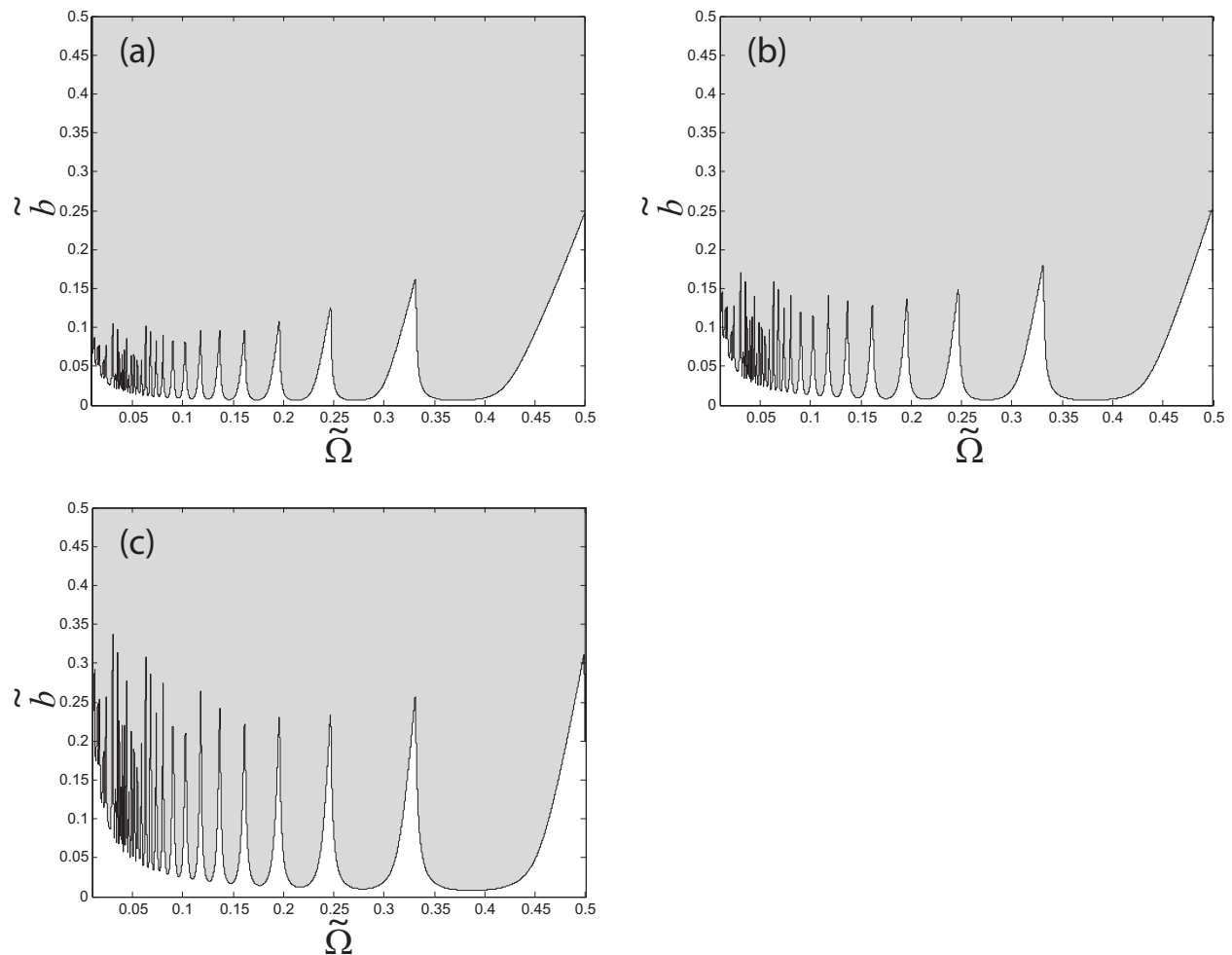
Fig. 8 Stability charts for the distributed force model of continuous turning plotted as a function of the nondimensionalized cutting speed and depth of cut. The damping ratio used is $\zeta = 0.0038$ and the delay ratios used are (_a_) $r = 0.03$, (_b_) $r = 0.05$, and (_c_) $r = 0.10$ (unstable regions shaded).

to the point force model when the delay ratio is very small, i.e., when the short delay is negligible compared with the discrete delay. However, for larger values of r, Fig. 8 shows an improved stability behavior at lower speeds.

3.2 Interrupted Turning Stability. For the point force model, Fig. 9 shows the cases when $\rho = 0.05$, 0.10, and 0.20, where ρ represents the fraction of the workpiece revolution that the tool is cutting. A fine mesh of 2400×600 was used to generate all the stability plots of interrupted turning. These results are in agreement with the results obtained in Ref. [24] for interrupted turning.

Figures 10 and 11 are stability charts for interrupted cutting, which use the distributed force model. In Fig. 10, cases (a)–(c) correspond to a value of $r = 0.001$. This low value of r yields similar results to those for the point force model (see Fig. 9). On the other hand, as the value of r increases to 0.03, as in cases (d)–(f), the stability at low speeds is improved for the different values of ρ. This trend is even more prominent in Fig. 11 where r was set to 0.05 and 0.10.

4 Discussion

This paper investigates the increased stability behavior commonly observed at low cutting speeds. In literature, this improved stability has been attributed to the interference between the workpiece and the tool relief face. The energy dissipation through this interference mechanism has been called process damping. On the

other hand, the distributed delay used in this paper has been an unmodeled parameter that was shown to have a great impact on low-speed cutting stability. More specifically, an exponential shape function is proposed to approximate the force distribution over the tool-chip contact length, and a constant delay ratio is introduced to describe the ratio between the distributed and the discrete delays.

The distributed force model results in a more complicated governing equation, a second-order delayed integrodifferential equation, that involves both a discrete and distributed delay. The distributed delay results from the finite time it takes the chip to slide along the rake face of the tool while the discrete delay is from the period between consecutive passages of the cutting tooth. An approach to transform the governing equation of motion into a third-order discrete system is described and the state-space representation of the new system is obtained. The state-space TFEA technique is then used to chart the stability boundaries for continuous and interrupted turning. Different delay ratios are used for generating stability charts to study the effect of the distributed delay on stability. For comparison purposes, the point force model is also used to obtain the conventional stability charts for continuous and interrupted turning. It was found that for a small value of the delay ratio, i.e., when the continuous delay is negligible in comparison to the discrete one, the predicted stability boundaries were similar to those of the point force model. However, for larger values of the delay ratio, the distributed force model showed an improved stability behavior at lower speeds when compared with
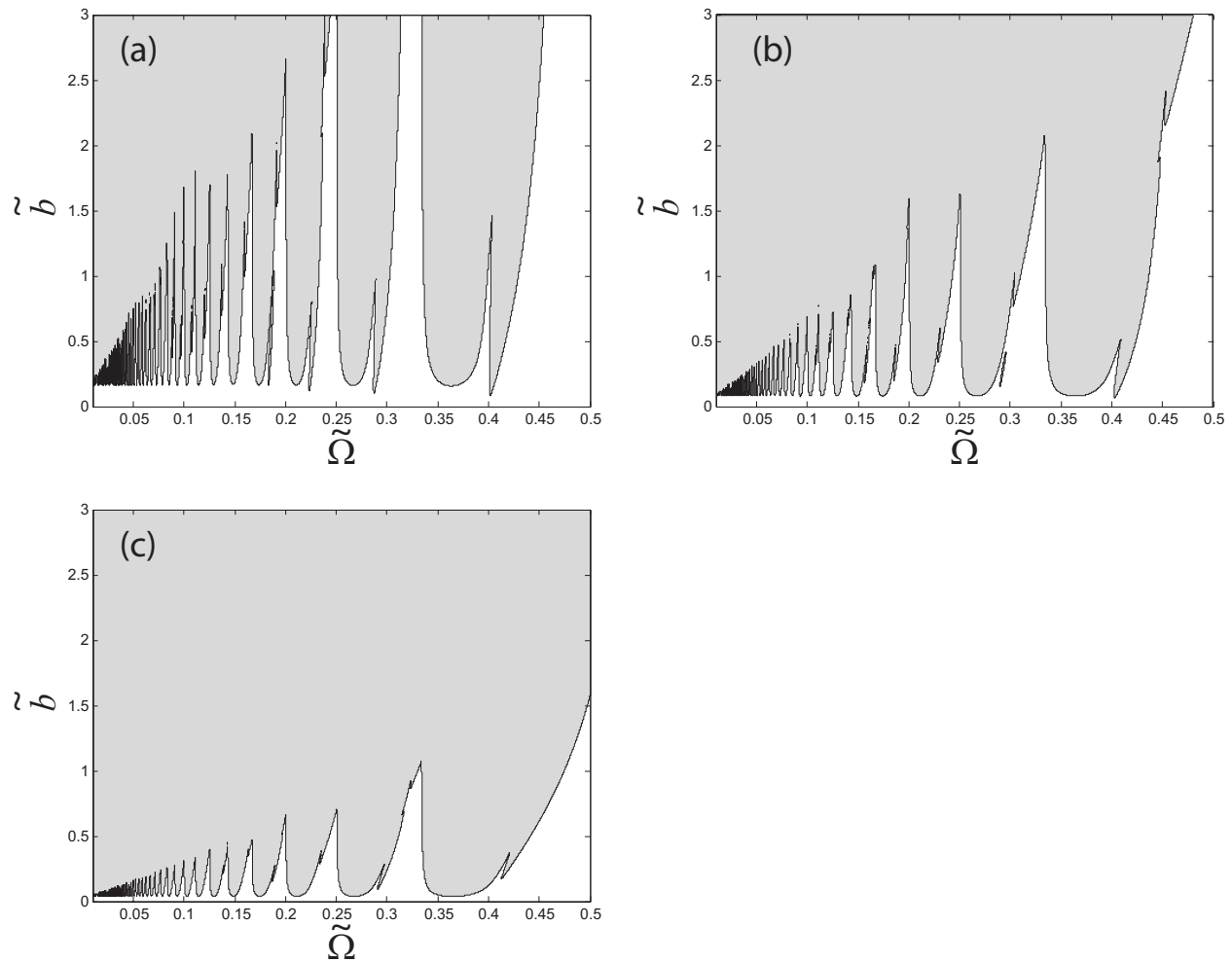
Fig. 9 Stability charts for the point force model of interrupted turning plotted as a function of the nondimensionalized cutting speed and depth of cut. The damping ratio used is $\zeta=0.0038$ and the cases for different fractions of the workpiece revolution that the tool is cutting are (*a*) $\rho=0.05$, (*b*) $\rho=0.10$, and (*c*) $\rho=0.20$ (unstable regions shaded).

the point force model. The stable parameter space continued to increase with increases in the delay ratio, which confirms the stabilizing effect of the distributed delay.

A specific contribution of the current paper is the introduction of a more realistic method to represent cutting forces. More specifically, the present manuscript has described and investigated an alternative physical explanation for process damping where a distributed cutting force model, along with an exponential distribution over the tool-chip interface, is assumed. Although a distributed force model is more realistic, this idea contrasts the standard approach of using a point force. The distributed force model also provides an alternative explanation for the improved stability at low speeds while still allowing analytical stability analysis. The current approach further averts the complications of previous works, which either uses an ad hoc damping term that is inversely proportional to spindle speed or a displaced volume relationship that must be numerically and experimentally calibrated. However, although the stability diagrams from the present study agree qualitatively with the observed low-speed stability results, the authors believe that only experimental investigations can reveal, which models or combination of models will most accurately capture the process damping effects.

Possible tasks for future research include experimental verification and/or comparison study with historical models of process damping. The success of the current approach in handling short delays also suggests that a similar analysis can be performed to accommodate interference forces on the relief face. This will still allow for an analytical stability analysis in the parameter space while capturing the physical phenomena of the process. Finally, another task is to construct a solution strategy that can accommodate different shape functions for the force distribution and to expand these solution techniques to other cutting operations.

Acknowledgment

Appendix: Interrupted Turning-Free Vibration

In order to establish the stability of an interrupted turning process, it is necessary to obtain the state transition matrix describing the system states during free vibration. The third-order system derived in the analysis of the distributed force model in Eq. (26) will be considered first since the transition matrix for the second-order system can be obtained easily from the third-order case. For a nondimensionalized third-order system, the equation of motion during free vibration is
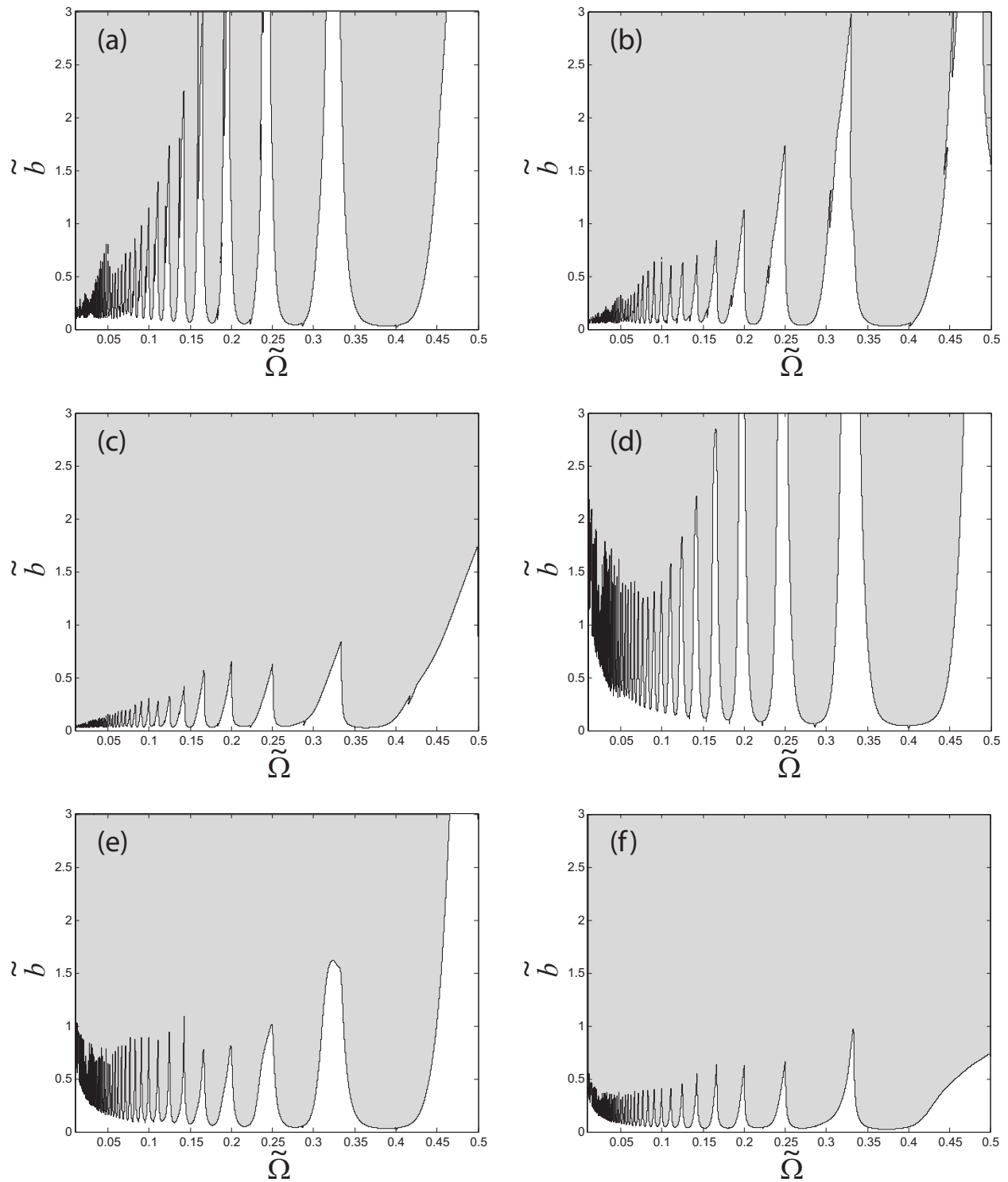
Fig. 10 Stability charts for the distributed force model of interrupted turning plotted as a function of the nondimensionalized cutting speed and depth of cut. The damping ratio used is $\zeta=0.0038$ and the cases for different fractions of the workpiece revolution that the tool is cutting and different delay ratios are (a) $\rho=0.05$ and $r=0.001$, (b) $\rho=0.10$ and $r=0.001$, (c) $\rho=0.20$ and $r=0.001$, (d) $\rho=0.05$ and $r=0.03$, (e) $\rho=0.10$ and $r=0.03$, and (f) $\rho=0.20$ and $r=0.03$ (unstable regions shaded).
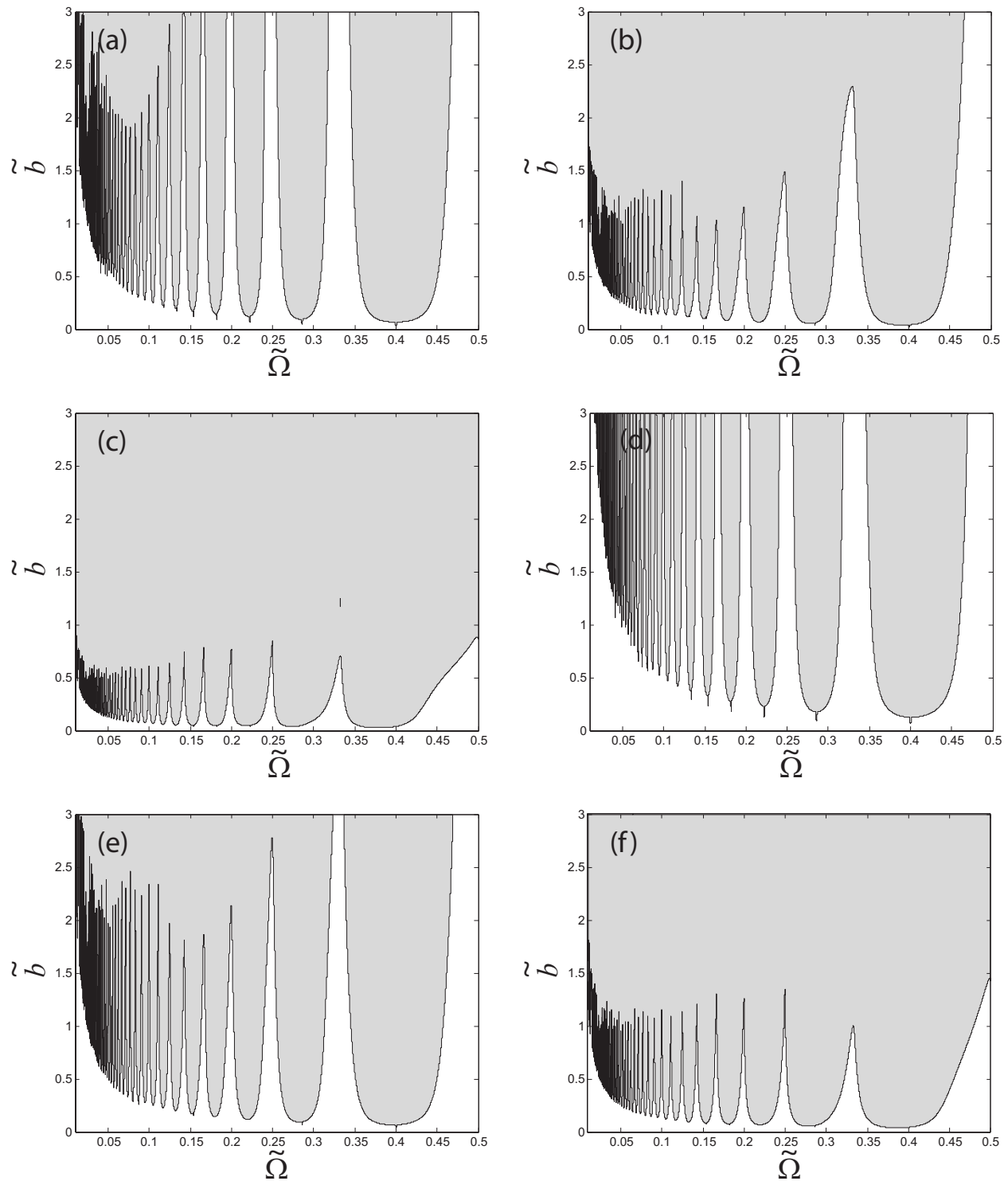
Fig. 11 Stability charts for the distributed force model of interrupted turning plotted as a function of the nondimensionalized cutting speed and depth of cut. The damping ratio used is $\zeta=0.0038$ and the cases for different fractions of the workpiece revolution that the tool is cutting and different delay ratios are (*a*) $\rho=0.05$ and $r=0.05$, (*b*) $\rho=0.10$ and $r=0.05$, (*c*) $\rho=0.20$ and $r=0.05$, (*d*) $\rho=0.05$ and $r=0.10$, (*e*) $\rho=0.10$ and $r=0.10$, and (*f*) $\rho=0.20$ and $r=0.10$ (unstable regions shaded).

$$\overset{(3)}{\xi}(t) + 2\zeta\ddot{\xi}(t) + \dot{\xi}(t) = 0 \qquad (A1)$$

which has the solution $\xi(t) = c_1 e^{\lambda_1 t} + c_2 e^{\lambda_2 t} + c_3$, where $\lambda_{1,2} = \zeta \pm \sqrt{\zeta^2 - 1}$. The solutions for the different states of the system can be expressed in matrix form as

$$\begin{bmatrix} \xi(t) \\ \dot{\xi}(t) \\ \ddot{\xi}(t) \end{bmatrix} = \begin{bmatrix} e^{\lambda_1 t} & e^{\lambda_2 t} & 1 \\ \lambda_1 e^{\lambda_1 t} & \lambda_2 e^{\lambda_2 t} & 0 \\ \lambda_1^2 e^{\lambda_1 t} & \lambda_2^2 e^{\lambda_2 t} & 0 \end{bmatrix} \begin{bmatrix} c_1 \\ c_2 \\ c_3 \end{bmatrix} \qquad (A2)$$

or equivalently

$$\boldsymbol{\xi}(t) = \mathbf{L}\mathbf{c} \qquad (A3)$$

Setting $t = t_c$ at the beginning of free vibration, and solving simultaneously for the set of initial conditions forming a 3×3 identity matrix, Eq. (A2) reads

$$\mathbf{I} = \mathbf{LC} \qquad (A4)$$

where the square matrix of coefficients, $\mathbf{C}$, can be found by inverting $\mathbf{L}$

$$\mathbf{C} = \mathbf{L}^{-1} = \begin{bmatrix} 0 & -\dfrac{\lambda_2}{\lambda_1(\lambda_1 - \lambda_2)}e^{-\lambda_1 t_c} & \dfrac{1}{\lambda_1(\lambda_1 - \lambda_2)}e^{-\lambda_1 t_c} \\ 0 & \dfrac{\lambda_1}{\lambda_2(\lambda_1 - \lambda_2)}e^{-\lambda_2 t_c} & -\dfrac{1}{\lambda_2(\lambda_1 - \lambda_2)}e^{-\lambda_2 t_c} \\ 1 & -\dfrac{(\lambda_1 + \lambda_2)}{(\lambda_1 \lambda_2)} & \dfrac{1}{(\lambda_1 \lambda_2)} \end{bmatrix} \qquad (A5)$$

Let t_f be the duration of free vibration, then a state transition matrix can be obtained that relates the state of the tool as it exits from the cut at $t = t_c$ to the state of the tool as it re-enters into the cut at $t = t_c + t_f$

$$\begin{bmatrix} \xi(t_c+t_f) \\ \dot{\xi}(t_c+t_f) \\ \ddot{\xi}(t_c+t_f) \end{bmatrix} = \begin{bmatrix} e^{\lambda_1(t_c+t_f)} & e^{\lambda_2(t_c+t_f)} & 1 \\ \lambda_1 e^{\lambda_1(t_c+t_f)} & \lambda_2 e^{\lambda_2(t_c+t_f)} & 0 \\ \lambda_1^2 e^{\lambda_1(t_c+t_f)} & \lambda_2^2 e^{\lambda_2(t_c+t_f)} & 0 \end{bmatrix} \begin{bmatrix} 0 & -\dfrac{\lambda_2}{\lambda_1(\lambda_1-\lambda_2)}e^{-\lambda_1 t_c} & \dfrac{1}{\lambda_1(\lambda_1-\lambda_2)}e^{-\lambda_1 t_c} \\ 0 & \dfrac{\lambda_1}{\lambda_2(\lambda_1-\lambda_2)}e^{-\lambda_2 t_c} & -\dfrac{1}{\lambda_2(\lambda_1-\lambda_2)}e^{-\lambda_2 t_c} \\ 1 & -\dfrac{(\lambda_1+\lambda_2)}{\lambda_1\lambda_2} & \dfrac{1}{(\lambda_1\lambda_2)} \end{bmatrix} \begin{bmatrix} \xi(t_c) \\ \dot{\xi}(t_c) \\ \ddot{\xi}(t_c) \end{bmatrix} \Rightarrow \begin{bmatrix} \xi(t_c+t_f) \\ \dot{\xi}(t_c+t_f) \\ \ddot{\xi}(t_c+t_f) \end{bmatrix} = \boldsymbol{\Phi} \begin{bmatrix} \xi(t_c) \\ \dot{\xi}(t_c) \\ \ddot{\xi}(t_c) \end{bmatrix} \qquad (A6)$$

where the state transition matrix $\boldsymbol{\Phi}$ is

$$\boldsymbol{\Phi} = \frac{1}{\lambda_1 - \lambda_2} \begin{bmatrix} (\lambda_1 - \lambda_2) & -\dfrac{\lambda_2}{\lambda_1}e^{\lambda_1 t_f} + \dfrac{\lambda_1}{\lambda_2}e^{\lambda_2 t_f} - \dfrac{(\lambda_1^2 - \lambda_2^2)}{(\lambda_1 \lambda_2)} & \dfrac{1}{\lambda_1}e^{\lambda_1 t_f} - \dfrac{1}{\lambda_2}e^{\lambda_2 t_f} + \dfrac{(\lambda_1 - \lambda_2)}{(\lambda_1 \lambda_2)} \\ 0 & \lambda_1 e^{\lambda_2 t_f} - \lambda_2 e^{\lambda_1 t_f} & e^{\lambda_1 t_f} - e^{\lambda_2 t_f} \\ 0 & \lambda_1 \lambda_2 e^{\lambda_2 t_f} - \lambda_1 \lambda_2 e^{\lambda_1 t_f} & \lambda_1 e^{\lambda_1 t_f} - \lambda_2 e^{\lambda_2 t_f} \end{bmatrix} \qquad (A7)$$

The 2×2 state transition matrix for the second-order system can be obtained by eliminating the first row and the first column in Eq. (A7) to obtain

$$\boldsymbol{\Phi} = \frac{1}{\lambda_1 - \lambda_2} \begin{bmatrix} \lambda_1 e^{\lambda_2 t_f} - \lambda_2 e^{\lambda_1 t_f} & e^{\lambda_1 t_f} - e^{\lambda_2 t_f} \\ \lambda_1 \lambda_2 e^{\lambda_2 t_f} - \lambda_1 \lambda_2 e^{\lambda_1 t_f} & \lambda_1 e^{\lambda_1 t_f} - \lambda_2 e^{\lambda_2 t_f} \end{bmatrix} \qquad (A8)$$

which agrees with the result obtained in Ref. [30].

References

[1] Tobias, S. A., and Fishwick, W., 1958, "Theory of Regenerative Machine Tool Chatter," The Engineer, **205**, pp. 16–23.
[2] Cook, N. H., 1959, "Self-Excited Vibrations in Metal Cutting," ASME J. Eng. Ind., **81**, pp. 183–186.
[3] Tlusty, J., and Polacek, M., 1963, "The Stability of Machine Tools Against Self-Excited Vibrations in Machining," *Proceedings of the ASME International Research in Production Engineering*, pp. 465–474.
[4] Merrit, H. E., 1965, "Theory of Self-Excited Machine-Tool Chatter, Contribution to Machine-Tool Chatter Research-1," ASME J. Eng. Ind., **87**, pp. 447–454.
[5] Boyer, R. R., 1996, "An Overview on the Use of Titanium in the Aerospace Industry," Mater. Sci. Eng., A, **213**(1–2), pp. 103–114.
[6] 2003, *Titanium and Titanium Alloys: Fundamentals and Applications*, C. Leyens and M. Peters, eds., Wiley-VCH, Weinheim, Germany.
[7] Sisson, T. R., and Kegg, R. L., 1969, "An Explanation of Low-Speed Chatter Effects," ASME J. Eng. Ind., **91**(4), pp. 951–958.
[8] Tlusty, J., and Heczko, O., 1980, "Improving Tests of Damping in the Cutting Process," *Proceedings of the Eighth North American Manufacturing Research Conference*, pp. 372–376.
[9] Balakrishnan, P., Eman, K. F., and Wu, S. M., 1981, "Analysis of Cutting Process Damping," *Proceedings of the Ninth North American Manufacturing Research Conference*, pp. 247–249.
[10] Tlusty, J., 1978, "Analysis of the State of Research in Cutting Dynamics," CIRP Ann., **27**(2), pp. 583–589.
[11] Minis, I., Magrab, E., and Pandelidis, I., 1990, "Improved Methods for the Prediction of Chatter in Turning, Part 2: Determination of Cutting Process Parameters," ASME J. Eng. Ind., **112**(1), pp. 21–27.
[12] Wu, D. W., 1988, "Application of a Comprehensive Dynamic Cutting Force Model to Orthogonal Wave-Generating Processes," Int. J. Mech. Sci., **30**(8), pp. 581–600.
[13] Jemielniak, K., and Widota, A., 1989, "Numerical Simulation of Non-Linear Chatter Vibration in Turning," Int. J. Mach. Tools Manuf., **29**(2), pp. 239–247.
[14] Shaw, M., and DeSalvo, G. J., 1970, "On the Plastic Flow Beneath a Blunt Axisymmetric Indenter," ASME J. Eng. Ind., **92**, pp. 480–494.
[15] Tarng, Y. S., Young, H. T., and Lee, B. Y., 1994, "An Analytical Model of Chatter Vibration in Metal Cutting," Int. J. Mach. Tools Manuf., **34**(2), pp. 183–197.
[16] Lee, B. Y., Tarng, Y. S., and Ma, S. C., 1995, "Modeling of the Process Damping Force in Chatter Vibration," Int. J. Mach. Tools Manuf., **35**(7), pp. 951–962.
[17] Chiou, R. Y., and Liang, S. Y., 1998, "Chatter Stability of a Slender Cutting Tool in Turning With Tool Wear Effects," Int. J. Mach. Tools Manuf., **38**(4), pp. 315–327.
[18] Clancy, B. E., and Shin, Y. C., 2002, "A Comprehensive Chatter Prediction Model for Face Turning Operation Including Tool Wear Effect," Int. J. Mach. Tools Manuf., **42**(9), pp. 1035–1044.
[19] Chandiramani, N. K., and Pothala, T., 2006, "Dynamics of 2-DOF Regenerative Chatter During Turning," J. Sound Vib., **290**, pp. 448–464.
[20] Stépán, G., 1989, *Retarded Dynamical Systems: Stability and Characteristic Functions*, Wiley, New York.
[21] Stépán, G., 1997, *Dynamics and Chaos in Manufacturing Processes*, F. Moon, ed., Wiley, New York, pp. 165–192.
[22] Mann, B. P., and Patel, B., "Stability of Delay Equations Written as State Space Models," J. Vib. Control (to be published).
[23] Jordan, D. W., and Smith, P., 1999, *Nonlinear Ordinary Differential Equations: An Introduction to Dynamical Systems*, 3rd ed., Oxford University Press, Oxford.
[24] Szalai, R., and Stépán, G., 2006, "Lobes and Lenses in the Stability Chart of Interrupted Turning," ASME J. Comput. Nonlinear Dyn., **1**, pp. 205–211.
[25] Altintas, Y., 2000, *Manufacturing Automation*, Cambridge University Press, New York.

[26] Zorev, N., 1963, "Inter-Relationship Between Shear Processes Occurring Along Tool Face and Shear Plane in Metal Cutting," *International Research in Production Engineering*, ASME, New York, pp. 42–49.

[27] Bailey, J. A., 1975, "Friction in Metal Machining—Mechanical Aspects," Wear, **31**, pp. 243–275.

[28] Arsecularatne, J. A., 1997, "On the Tool-Chip Interface Stress Distributions, Ploughing Force and Size Effect in Machining," Int. J. Mach. Tools Manuf., **37**(7), pp. 885–899.

[29] Madhavan, V., Chandrasekar, S., and Farris, T. N., 2002, "Direct Observations of the Chip-Tool Interface in the Low Speed Cutting of Pure Metals," ASME J. Tribol., **124**, pp. 617–626.

[30] Mann, B. P., and Young, K. A., 2006, "An Empirical Approach for Delayed Oscillator Stability and Parametric Identification," Proc. R. Soc. London, Ser. A, **462**, pp. 2145–2160.

[31] Bayly, P. V., Halley, J. E., Mann, B. P., and Davis, M. A., 2003, "Stability of Interrupted Cutting by Temporal Finite Element Analysis," ASME J. Manuf. Sci. Eng., **125**, pp. 220–225.